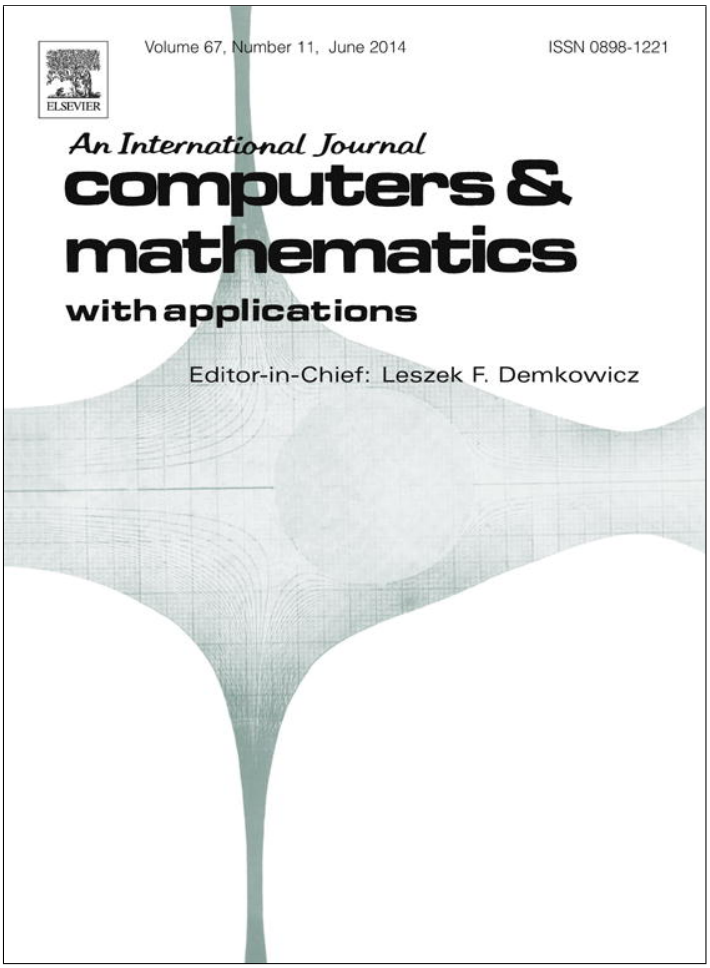

Computers and Mathematics with Applications 67 (2014) 2029–2040

Contents lists available at ScienceDirect

Computers and Mathematics with Applications

journal homepage: www.elsevier.com/locate/camwa

Extension of a second order velocity slip/temperature jump boundary condition to simulate high speed micro/nanoflows

Seyed Ali Rooholghdos, Ehsan Roohi *

High Performance Computing (HPC) Laboratory, Department of Mechanical Engineering, Ferdowsi University of Mashhad, P.O. Box 91775-1111, Mashhad, Iran

ARTICLE INFO

Article history:
Received 29 November 2013
Received in revised form 26 March 2014
Accepted 3 May 2014
Available online 19 May 2014

Keywords:
Finite element technique
Rarefied flow
Second order slip/jump boundary conditions
Petrov–Galerkin method
Non-equilibrium flow
Micro/nanoflows

ABSTRACT

In the current work, for the first time, we extend the application of a second order slip/jump equations introduced by Karniadakis et al. for the simulation of high speed, high Knudsen (Kn) number flows over a nano-scale flat plate and a micro-scale cylinder. The NS equations subject to a second order slip/jump boundary conditions are solved using the Petrov–Galerkin Finite Element discretization. We compare our numerical solution for flow and thermal field with the solution of the DSMC and Generalized Hydrodynamic (GH) techniques, as well as a recently developed slip/jump boundary condition, i.e., Paterson equation. Current results demonstrate the suitable accuracy of the employed boundary conditions for different set of test cases. Our numerical solutions are obtained with much less numerical costs compared to alternative boundary conditions.

1. Introduction

During the last decades, the use of micro/nano electromechanical systems (MEMS/NEMS) has been significantly increased in various industries [1]. The low-pressure gas flow or small length scale which is present in micro/nanofluidics devices results in flow rarefication. Consequently, the departure from thermodynamic equilibrium due to the rarefication makes the Navier–Stokes (NS) equations invalid. The degree of gas rarefication is determined by the Knudsen number, defined as follows:

$$Kn = \frac{\lambda}{L} \tag{1}$$

where λ and L are the mean free path and characteristic length of the geometry, respectively. With regard to the values of the Knudsen number, the gas flows are classified as the continuum regime ($Kn < 10^{-3}$), slip flow regime ($10^{-3} < Kn < 10^{-1}$), transition regime ($10^{-1} < Kn < 10$), and free molecular flow ($Kn > 10$). The gas flow can be simulated using the Boltzmann equation in all regimes while the NS equations can be used only in continuum regimes. Nevertheless, we can still simulate the rarefied gas flow with the NS equations in the slip flow regime and slightly beyond provided that no-slip boundary conditions are replaced with velocity slip and temperature jump boundary conditions. Alternatively, moment methods have been widely employed for rarefied gas flows [2–4]. The benefit of moment methods is high accuracy and low computational costs [5]. Recently, boundary conditions (BC) for the regularized 13 moments equations were also extended to derive second order BCs for the NS equations [5].

* Corresponding author. Tel.: +98 511 8805136; fax: +98 511 8763304.
E-mail address: e.roohi@ferdowsi.um.ac.ir (E. Roohi).

http://dx.doi.org/10.1016/j.camwa.2014.05.004
0898-1221/

Eu [6] demonstrated that the high Mach number effects also contribute in non-equilibrium besides rarefication. He introduced a combined parameter that considers both of the rarefaction and compressibility factors. This parameter is defined as:

$$N_\delta = KnM\sqrt{\frac{2\gamma}{\pi}}. \tag{2}$$

To consider the effects of flow rarefactions near the walls, a first-order accurate velocity slip boundary condition was derived for the first time by Maxwell [7]:

$$U_s - U_w = \left(\frac{2-\sigma_v}{\sigma_v}\right) Kn \frac{\partial U_s}{\partial n} \tag{3}$$

where σ_v and σ_T represent the momentum and thermal accommodation coefficients, respectively. Similarly, Smoluchowski proposed a first-order temperature jump condition with the following equation [8]:

$$T_s - T_w = \left(\frac{2-\sigma_T}{\sigma_T}\right)\left(\frac{2\gamma}{\gamma+1}\right)\frac{Kn}{Pr}\frac{\partial T}{\partial n}. \tag{4}$$

Generally, slip/jump boundary conditions can be classified according to their accuracy and limits of applicability. The first-order slip boundary conditions can be expressed as in the following general form [9]:

$$U_s - U_w = C_1 Kn \left(\frac{\partial U}{\partial n}\right)_s \tag{5}$$

where C_1 represents first-order slip coefficient, i.e., $C_1 = \frac{2-\sigma_v}{\sigma_v}$ in Maxwell's condition. Different values have been proposed for this coefficient based on various analytical, numerical or experimental approaches. For example, see Loyalka et al. [10], Bohukudumbi et al. [11], Karniadakis et al. [12] and Agrawal et al. [13].

When rarefication increases, more accurate boundary conditions are required. Similar to the aforementioned general equation, the following equation can be considered for the second-order slip condition:

$$U_s - U_w = C_1 Kn \left(\frac{\partial U}{\partial n}\right)_s - C_2 Kn^2 \left(\frac{\partial^2 U}{\partial n^2}\right)_s \tag{6}$$

where C_1 and C_2 are the first-order and second-order coefficients. Different magnitudes have been proposed for the following coefficients based on the experimental or theoretical approaches. For example, see Refs. [14–18]. In addition to the following equation, another type of slip/jump boundary condition, Langmuir type, has been presented considering the condensation of gas molecules on the surface. Eu et al. [19] and Myong [20–22] developed this family of boundary conditions.

2. Karniadakis boundary condition

Karniadakis et al. [12] derived a second-order accurate slip/jump boundary condition based on the kinetic theory of gases. They calculated mean tangential velocity of the gas molecules and temperature jump boundary conditions as follows [12]:

$$u_s = \frac{1}{2}\left[u_\lambda + (1-\sigma_v)\, u_\lambda + \sigma_v u_w\right] \tag{7}$$

$$T_s = \left(\frac{(2-\sigma_T)}{Pr}\frac{2\gamma}{(\gamma+1)}T_\lambda + \sigma_T T_w\right) \Big/ \left(\sigma_T + \frac{2\gamma}{(\gamma+1)}\frac{(2-\sigma_T)}{Pr}\right) \tag{8}$$

where the subscripts λ and w denote value of the variables calculated at a distance proportional to the mean-free-path away from the surface and at the surface, respectively. Karniadakis et al. [12] showed that the Taylor expansion of Eq. (7) results in a second order BC in terms of Kn number; therefore, this BC is called the second order in the current paper.

Karniadakis et al. [12] reported that the best agreement with the DSMC solution for micro-channel geometry was obtained if u_λ and T_λ were calculated at a distance equal to one mean free path away from the wall. In the current work, a sensitivity analysis was performed for employment of Eqs. (7)–(8) for external flow geometries. We observed that best agreement with the DSMC solutions for velocity and temperature field is obtained if we calculate u_λ and T_λ at distances equal to λ and 2λ, respectively. σ_v and σ_T are the tangential momentum and energy accommodation coefficients. In addition, all of the variables are non-dimensionalized with the reference quantities in the freestream.

Contrary to most other common slip/jump boundary conditions, these boundary conditions are independent of calculating any velocity or temperature derivatives at the surface. Karniadakis et al. [12] noted that explicit implementation of boundary conditions which needs to calculate velocity or temperature gradients at the surface may result in unstable results. This reason along with high computational cost and numerical difficulties that come from calculating the higher order gradients encourage the researcher to focus on non-gradient slip/jump boundary conditions. In the current work, for the first time, we extend the applicability of Eqs. (7)–(8) for simulation of high speed external rarefied micro/nano flows.

Previous applications of these equations were limited to low speed internal flows [12,23]. We show that suitable accuracy of the above equations justifies the use of these equations for high speed non-equilibrium flows.

We used an explicit implementation of the above slip/jump boundary conditions as follows:

$$u_s^{n+1} = \frac{1}{2}\left[u_\lambda + (1-\sigma_v)\,u_\lambda + \sigma_v u_w\right]^n \tag{9}$$

$$T_s^{n+1} = \left[\left(\frac{(2-\sigma_T)}{Pr}\frac{2\gamma}{(\gamma+1)}T_\lambda + \sigma_T T_w\right) \Big/ \left(\sigma_T + \frac{2\gamma}{(\gamma+1)}\frac{(2-\sigma_T)}{Pr}\right)\right]^n. \tag{10}$$

Therefore, flow parameters needed in Eqs. (9) and (10) are known from the last iteration.

3. Finite element formulation

A Petrov–Galerkin finite element method is used to solve the compressible NS equations. This method is based on introducing and using an artificial diffusion which is applied locally along the streamlines. Simplicity, stability and high accuracy of this method are determinative factors for its usage [24]. The algorithm is implemented using bilinear quadrilateral elements. The NS equations can be written in the dimensionless forms as follows:

$$\begin{cases} \dfrac{\partial \rho}{\partial t} + \boldsymbol{u}\cdot\nabla\rho + \rho\nabla\cdot\boldsymbol{u} = 0 \\ \rho\left(\dfrac{\partial \boldsymbol{u}}{\partial t} + \boldsymbol{u}\cdot\nabla\boldsymbol{u}\right) + \dfrac{1}{\gamma M_\infty^2}\nabla p = \nabla\cdot\boldsymbol{\tau} \\ \rho\left(\dfrac{\partial E}{\partial t} + \boldsymbol{u}\cdot\nabla E\right) + (\gamma-1)\,\nabla\cdot(p\boldsymbol{u}) \\ \quad = \dfrac{\gamma}{Pr\times Re_\infty}\nabla\cdot\mu\left[\nabla E - \dfrac{(\gamma-1)}{2}\gamma M_\infty^2\nabla(\boldsymbol{u}\cdot\boldsymbol{u})\right] + \gamma(\gamma-1)M_\infty^2\nabla\cdot(\boldsymbol{\tau}\cdot\boldsymbol{u}) \end{cases} \tag{11}$$

where Re_∞ and M_∞ are respectively the Reynolds and Mach numbers defined at the reference conditions. $\boldsymbol{\tau}$ is the dimensionless deviatoric stress tensor.

The Petrov–Galerkin weak formulations of governing equations are written as:

$$\int_\Omega \left\{\omega\frac{\partial\rho}{\partial t} + v_\rho\left[u\frac{\partial\rho}{\partial x} + v\frac{\partial\rho}{\partial y}\right] + \omega\rho\left(\frac{\partial u}{\partial x} + \frac{\partial v}{\partial y}\right)\right\} d\Omega = 0 \tag{12}$$

$$\begin{aligned}&\int_\Omega \left\{\omega\rho\frac{\partial u}{\partial t} + v_u\rho\left(u\frac{\partial u}{\partial x} + v\frac{\partial u}{\partial y}\right) + \omega\frac{1}{\gamma M_\infty^2}\frac{\partial(\rho e)}{\partial x} + \frac{\mu}{Re_\infty}\left[\frac{\partial\omega}{\partial x}\left(\frac{4}{3}\frac{\partial u}{\partial x} - \frac{2}{3}\frac{\partial v}{\partial y}\right) + \frac{\partial\omega}{\partial y}\left(\frac{\partial u}{\partial y} + \frac{\partial v}{\partial x}\right)\right]\right\} d\Omega \\ &- \int_\Gamma \omega\frac{\mu}{Re_\infty}\left[\left(\frac{4}{3}\frac{\partial u}{\partial x} - \frac{2}{3}\frac{\partial v}{\partial y}\right)n_x + \left(\frac{\partial u}{\partial y} + \frac{\partial v}{\partial x}\right)n_y\right] d\Gamma = 0\end{aligned} \tag{13}$$

$$\begin{aligned}&\int_\Omega \left\{\omega\rho\frac{\partial v}{\partial t} + v_v\rho\left(u\frac{\partial v}{\partial x} + v\frac{\partial v}{\partial y}\right) + \omega\frac{1}{\gamma M_\infty^2}\frac{\partial(\rho e)}{\partial y} + \frac{\mu}{Re_\infty}\left[\frac{\partial\omega}{\partial x}\left(\frac{\partial u}{\partial y} + \frac{\partial v}{\partial x}\right) + \frac{\partial\omega}{\partial y}\left(\frac{4}{3}\frac{\partial v}{\partial y} - \frac{2}{3}\frac{\partial u}{\partial x}\right)\right]\right\} d\Omega \\ &- \int_\Gamma \omega\frac{\mu}{Re_\infty}\left[\left(\frac{\partial u}{\partial y} + \frac{\partial v}{\partial x}\right)n_x + \left(\frac{4}{3}\frac{\partial v}{\partial y} - \frac{2}{3}\frac{\partial u}{\partial x}\right)n_y\right] d\Gamma = 0\end{aligned} \tag{14}$$

$$\begin{aligned}&\int_\Omega \left\{\omega\rho\frac{\partial e}{\partial t} + v_e\rho\left(u\frac{\partial e}{\partial x} + v\frac{\partial e}{\partial y}\right) + \omega(\gamma-1)(\rho e)\left(\frac{\partial u}{\partial x} + \frac{\partial v}{\partial y}\right)\right. \\ &+ \omega\gamma(\gamma-1)\frac{M_\infty^2}{Re_\infty}\mu\left[\frac{4}{3}\left[\left(\frac{\partial u}{\partial x}\right)^2 + \left(\frac{\partial v}{\partial y}\right)^2 - \left(\frac{\partial u}{\partial x}\frac{\partial v}{\partial y}\right)\right] + \left(\frac{\partial u}{\partial y}\right)^2 + \left(\frac{\partial v}{\partial x}\right)^2 + 2\left(\frac{\partial u}{\partial y}\frac{\partial v}{\partial x}\right)\right] \\ &\left. + \frac{\gamma}{PrRe_\infty}\mu\left(\frac{\partial\omega}{\partial x}\frac{\partial e}{\partial x} + \frac{\partial\omega}{\partial y}\frac{\partial e}{\partial y}\right)\right\} d\Omega - \int_\Gamma \omega\left[\frac{\gamma}{PrRe_\infty}\mu\left(\frac{\partial e}{\partial x}n_x + \frac{\partial e}{\partial y}n_y\right)\right] d\Gamma = 0\end{aligned} \tag{15}$$

where Ω is open-connected domain, Γ is the boundary, n is the normal unit vector and v_ρ, v_u, v_e, and v_e that appeared in continuity, momentums and energy equations are Petrov–Galerkin weighting functions used in connective terms only. ω is the standard Galerkin weighting function which is equal to shape functions. Calculation of these parameters is described in detail in Ref. [24].

The weighting functions are calculated using the following equations [25]:

$$v_\rho = w + \frac{h}{2U}\left(u\frac{\partial w}{\partial x} + v\frac{\partial w}{\partial y}\right) \tag{16}$$

$$v_u = w + \alpha_u \frac{h}{2U}\left(u\frac{\partial w}{\partial x} + v\frac{\partial w}{\partial y}\right) \tag{17}$$

where

$$\alpha_u = \coth\left(\frac{\gamma_u}{2}\right) - \frac{2}{\gamma_u} \tag{18}$$

and

$$\gamma_u = \frac{\rho Re_\infty Uh}{\mu\left(1 + \frac{u^2}{3(u^2+v^2)}\right)} \tag{19}$$

$$v_v = w + \alpha_v \frac{h}{2U}\left(u\frac{\partial w}{\partial x} + v\frac{\partial w}{\partial y}\right) \tag{20}$$

where

$$\alpha_u = \coth\left(\frac{\gamma_v}{2}\right) - \frac{2}{\gamma_v} \tag{21}$$

and

$$\gamma_v = \frac{\rho Re_\infty Uh}{\mu\left(1 + \frac{v^2}{3(u^2+v^2)}\right)} \tag{22}$$

$$v_e = w + \alpha_e \frac{h}{2U}\mu\left(u\frac{\partial w}{\partial x} + v\frac{\partial w}{\partial y}\right) \tag{23}$$

where

$$\alpha_e = \coth\left(\frac{\gamma_e}{2}\right) - \frac{2}{\gamma_e} \tag{24}$$

and

$$\gamma_v = \frac{\rho Pr Re_\infty Uh}{\mu\gamma} \tag{25}$$

h is the element length associated with the mesh and direction of $\boldsymbol{u}$ [25].

We used a quadrilateral bilinear element, where the distributions of dependent variables in the interior of the elements are computed from the following equations:

$$\left.\begin{aligned} \rho(x,t) &= \sum_{i=1}^{n} N^i(x)\rho_i(t) \\ u(x,t) &= \sum_{i=1}^{n} N^i(x)u_i(t) \\ v(x,t) &= \sum_{i=1}^{n} N^i(x)v_i(t) \\ e(x,t) &= \sum_{i=1}^{n} N^i(x)e_i(t) \end{aligned}\right\}, \tag{26}$$

where $\psi_i(t) = \rho(t),\ u(t),\ v(t),\ e(t)$ is the value of variable ψ in ith node in time t. To obtain u_λ and T_λ once the mean-free-path was smaller than the element size, we applied a linear interpolation between the values of variables in the node located on the wall and the upper node.

Variations of the viscosity with the temperature are considered as follows:

$$\mu = \mu_{\text{ref}}\left(\frac{T}{T_{\text{ref}}}\right)^{\omega}, \qquad \mu_{\text{ref}} = \frac{15\sqrt{\pi mkT_{\text{ref}}}}{2\pi d_{\text{ref}}^2(5-2\omega)(7-2\omega)}. \tag{27}$$

For argon gas molecules, $T_{\text{ref}} = 273$ K, $d = 4/17 \times 10^{-10}$ (m), $\omega = 0.81$, $\mu_{\text{ref}} = 2.117 \times 10^{-5}$ [26].

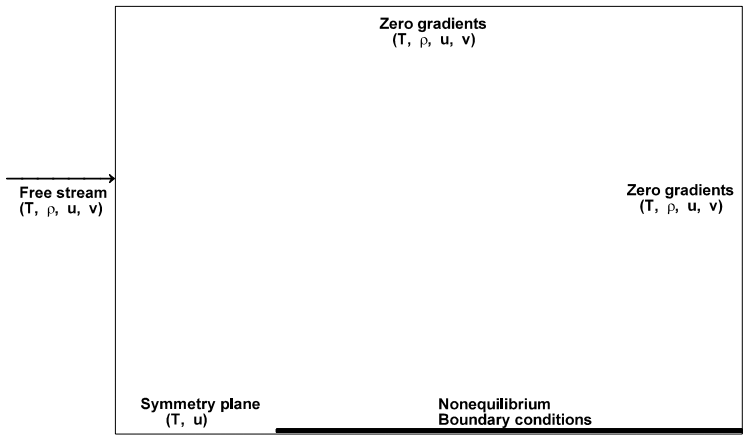

Fig. 1. Flat plate geometry and imposed boundary conditions.

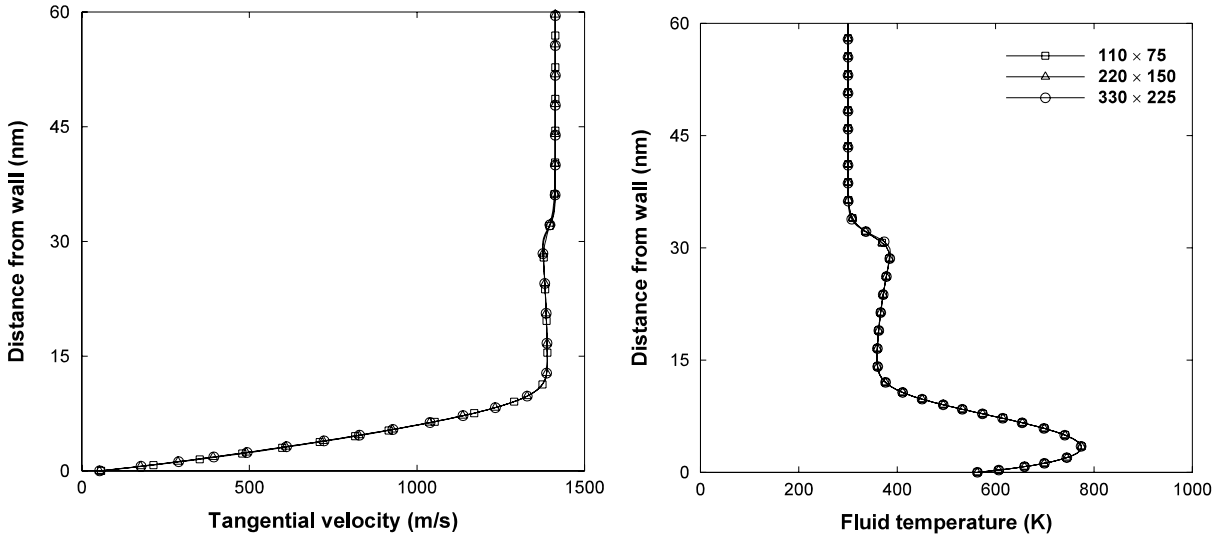

Fig. 2. Grid independency test.

4. Numerical results

4.1. Test 1: $Mach = 4.38$, $Kn = 0.0013$ *flow over the flat plate [26]*

In order to evaluate the accuracy of the Karniadakis et al. [12] slip/jump boundary conditions for high speed rarefied flows, three test cases have been considered over a wide range of flow non-equilibrium conditions. Firstly, we consider a supersonic flow of argon over a nano-scale flat plate [27]. The freestream flow conditions are $T_\infty = 300$ K and $p_\infty = 4.14 \times 10^7$ Pa. The plate has a length of 100 nm and is held at a constant temperature of $T_w = 500$ K. The inlet Mach and Knudsen numbers are respectively 4.38 and 0.0013 based on the freestream conditions and plate length, respectively. The value of Eu's parameter at the free stream conditions is $N_\delta = 0.00582$. In order to obtain a correct velocity distribution at the inlet of the plate, the inflow boundary is placed at a distance of 10% of the plate length from the leading edge. The height of the computational domain is 75 nm. Fig. 1 shows the geometry and boundary conditions. Since we assumed that molecules are reflected from the wall diffusively, both of the accommodation coefficients are set equal to one.

To obtain a grid independent solution, three different sets of grids, i.e., 110×75, 220×150 and 330×225, using bilinear quadrilateral elements were used. An expansion coefficient of 1.016 was used to increase the cell spacing in both axial and vertical directions. As Fig. 2 shows, all three grids provide almost identical solutions for tangential velocity and temperature at $x = 90$ nm. Therefore, we chose the grid with 110×75 cells which required less computational cost.

The convergence criterion is:

$$\frac{\left\| \boldsymbol{X}^{n+1} - \boldsymbol{X}^{n} \right\|}{\left\| \boldsymbol{X}^{n} \right\|}. \tag{28}$$

The convergence is achieved if the maximum of the relative error, defined by Eq. (15), of the dependent variables falls below the threshold value of 10^{-8}. We compare our results with the DSMC solution obtained using the dsmcFoam solver available in the OpenFOAM package [28].

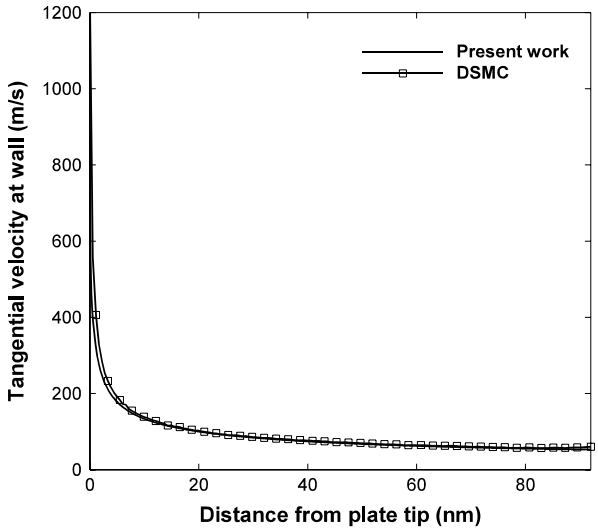

Fig. 3. Tangential velocity profile along the surface of the nano-scale flat plate ($M = 5.48$, $Kn = 0.0013$, $N_\delta = 0.00582$).

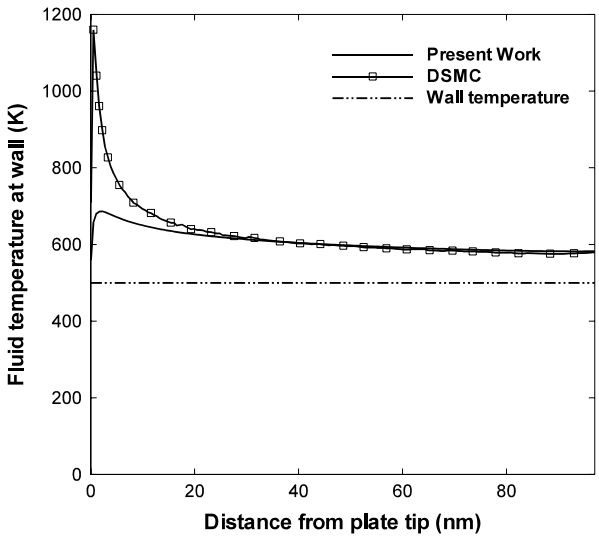

Fig. 4. Temperature profile along the surface of the nano-scale flat plate ($M = 5.48$, $Kn = 0.0013$, $N_\delta = 0.00582$).

Figs. 3 and 4 compare present results for the velocity and temperature distributions along the surface of the plate with the DSMC solution, respectively. Considering the surface velocity, Karniadakis's BCs results are almost coincident with the DSMC data over the whole plate including the shock and boundary layer regions. However, temperature jump deviates from the DSMC data in regions close to the leading edge, but this difference decreases when flow moves away from the beginning of the plate. This difference can perhaps be explained by the fact that DSMC particles returning to the inlet boundary could detect the shock formation while in the NS equations, the flow does not observe the plate until it reaches the plate tip [29].

Figs. 5–6 illustrate tangential velocity and temperature profiles at $x = 80$ nm. It is observed that there is reasonably good agreement between the current approach and DSMC. The mean absolute percentage error between the DSMC and NS solution for T and V are around 5.2% and 2.9%, respectively.

4.2. Test 2: $Mach = 12.7$, $Kn = 0.00418$ *flow over the flat plate [29]*

The second problem considered is the high speed hypersonic argon flow over a flat plate at Mach 12.7 and Knudsen number 0.00418. Eu's parameter for this problem at the free stream condition is $N_\delta = 0.0547$. Free-stream flow conditions are $T_\infty = 64.5$ K, $U_\infty = 1893.7$ (m/s), $p_\infty = 3.73$ Pa and $T_w = 292$ K. The mesh used for this case is the same as the previous test case. We compared our results with the DSMC data and Patterson BC's results reported in Ref. [29]. Greenshields and Reese [29] derived Patterson equations based on Grad's moment method. They showed that the results using Patterson's temperature jump BC compare quite well with the DSMC and are consistently better than those using the Smoluchowski temperature jump BC. Fig. 7 presents a comparison of the velocity distribution along the surface of the plate obtained by the DSMC as well as the NS equations using different BC's such as the Maxwell, Paterson and Karniadakis et al. model. As can

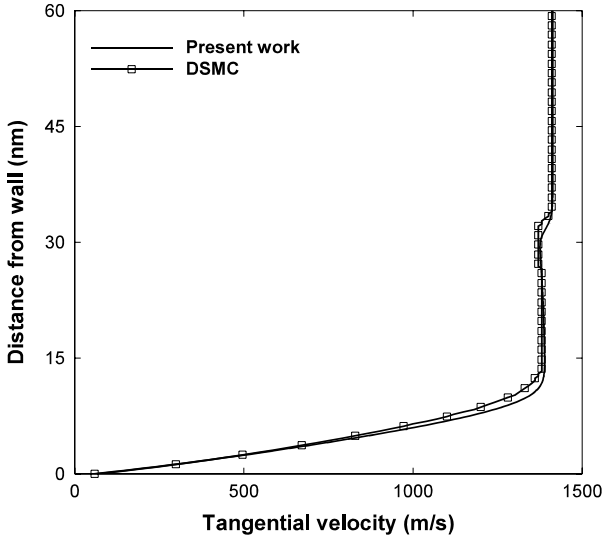

Fig. 5. Tangential velocity profile at $x = 80$ nm from the plate tip ($M = 5.48$, $Kn = 0.00129$, $N_\delta = 0.00582$).

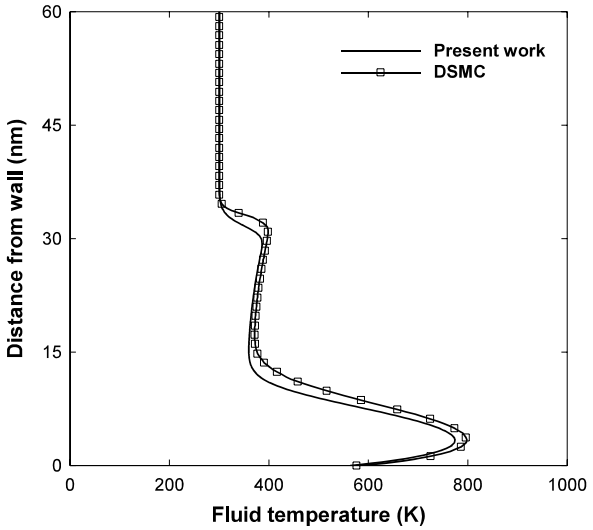

Fig. 6. Temperature profile at $x = 80$ nm from the plate tip ($M = 5.48$, $Kn = 0.00129$, $N_\delta = 0.00582$).

Table 1
Mean absolute percentage error for velocity slip over the whole surface.

BC	Present work	Patterson	Maxwell
MAPE	34.23%	84.14%	89.457%

be deduced from this figure, Karniadakis et al.'s BC predicts the closest results to the DSMC data and performs considerably better than the Paterson model, which coincides with the Maxwell model for this test case.

Fig. 8 shows a comparison of the temperature distribution along the surface of the plate. As observed in this figure, the solution of the present model coincides with Patterson's BCs, and both boundary conditions give better results for the surface temperature than the Smoluchowski condition. Similar to Fig. 4, CFD and DSMC solutions are different at the beginning of the flat plate while they approach each other as flow goes further along the plate. The mean absolute percentage error (MAPE) for velocity slip and temperature jump over the whole surface is reported in Tables 1–2.

$$\text{MAPE} = \frac{1}{n}\sum_{t=1}^{n}\left|\frac{X_{\text{DSMC}} - X_{NS}}{X_{\text{DSMC}}}\right| \tag{29}$$

where n is the number of cells and X is the quantity of interest.

Additionally, profiles of the temperature and tangential velocity at $x = 25$ mm are presented in Figs. 9–10, respectively. From Fig. 9, we observe that almost all BC models predict a higher value of slip on the plate in comparison with the DSMC solutions while they agree with the DSMC solution from slightly above the plate until $y < 1$ mm. Deviation between DSMC

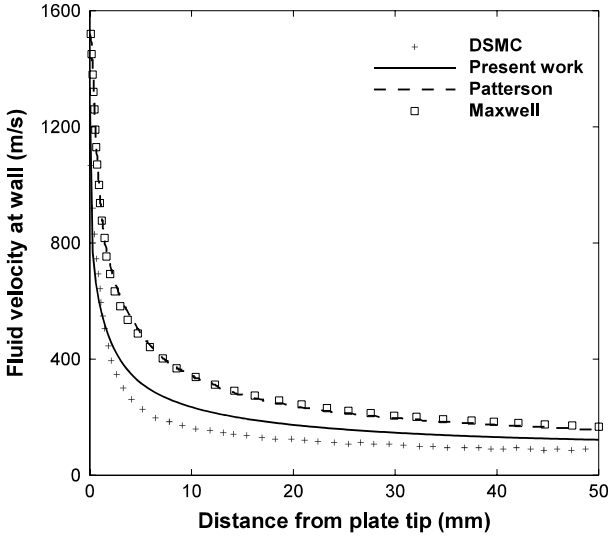

Fig. 7. Velocity profile along the surface of the flat plate ($M = 12.7$, $Kn = 0.00418$, $N_\delta = 0.0547$).

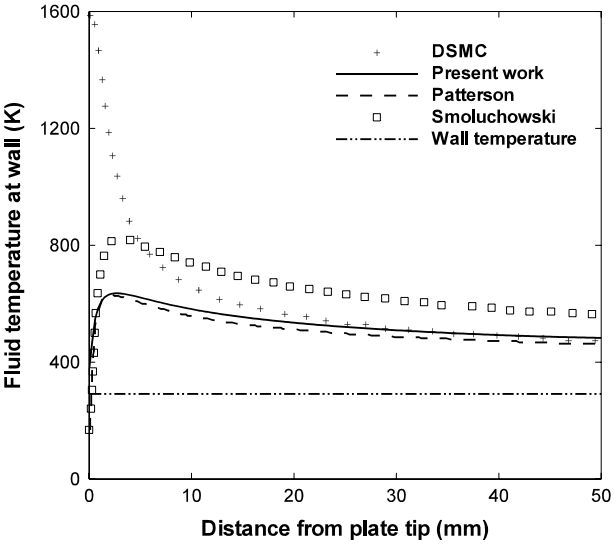

Fig. 8. Temperature profile along the surface of the flat plate ($M = 12.7$, $Kn = 0.00418$, $N_\delta = 0.0547$).

Table 2
Mean absolute percentage error for temperature jump over the whole surface.

BC	Present work	Patterson	Smoluchowski
MAPE	8.80%	13.97%	19.6%

and BC's increases until flow arrives around at $y = 5$ mm. From Fig. 10, we observe that Karniadakis et al.'s BC predicts temperature at the surface 7% less than DSMC, and almost equal to the Patterson BC. It is observed that DSMC data reaches a peak, where the value of temperature is about 1100 K, at 1.2 mm away from the wall surface. In this region, the closest solution to the DSMC data belongs to Smoluchowski, Karniadakis, and Patterson BCs, respectively. From $y > 3$ mm, Paterson solution becomes closer to the DSMC data while around $y = 6.8$, Karniadakis and Smoluchowski models agree better with the DSMC data. Overall, the mean absolute percentage errors for Paterson, Karniadakis and Smoluchowski models are respectively 14.49%, 16.68% and 19.5%.

4.3. Test 3: $Mach = 5.48$, $Kn = 0.05$ *flow over the cylinder [30]*

The third problem considered in this work is the hypersonic argon flow past a cylinder at Mach 5.48 and Knudsen number (based on radius of cylinder) 0.05. Eu's parameter at freestream conditions is $N_\delta = 0.2823$. The freestream flow temperature is $T_\infty = 26.6$ K. Also, the surface temperature of the circular cylinder is fixed at 293 K. Fig. 11 shows computational domain and relevant boundary conditions employed for our numerical simulation. A structured grid with 240×150 nodes

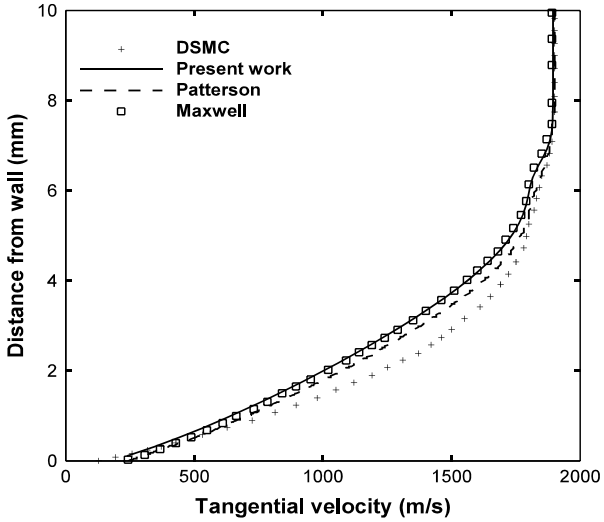

Fig. 9. Tangential velocity profile at $x = 25$ mm from the plate tip ($M = 12.7$, $Kn = 0.00418$, $N_\delta = 0.0547$).

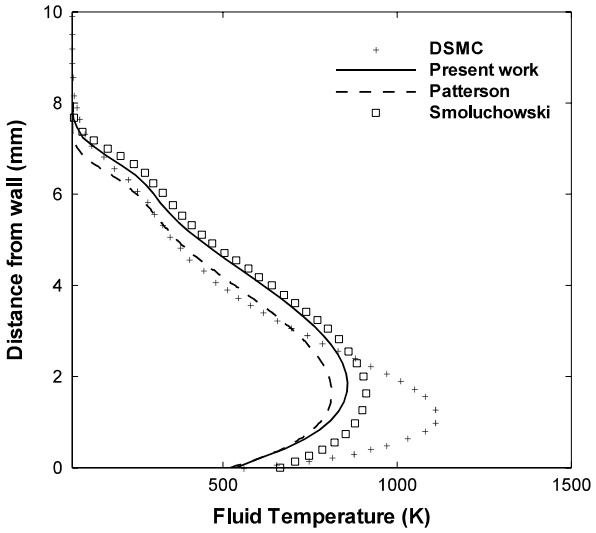

Fig. 10. Temperature profile at $x = 25$ mm from the plate tip ($M = 12.7$, $Kn = 0.00418$, $N_\delta = 0.0547$).

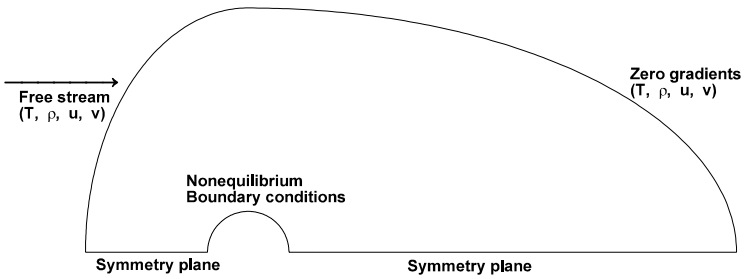

Fig. 11. Geometry and boundary conditions.

that corresponds to 36,000 bilinear quadrilateral elements is used. Our results are compared with the DSMC data [30,31], Generalized Hydrodynamic model results [32], and results computed using the nonlinear Boltzmann equations [33]. In Fig. 12, distributions of the normalized density, velocity and pressure (with respect to the freestream flow conditions) along the stagnation line are plotted. The distance is normalized using mean free path of the free stream flow.

It is observed that the Karniadakis BC gives reasonably good prediction for flow properties especially close to the surface of the cylinder, i.e., although there is some difference between CFD results and other approaches in the shock wave region, post-shock properties of the current simulation agree with the DSMC and Boltzmann solutions. This observation is in agreement with the finding reported in Ref. [34]. Fig. 13 shows the contour of density and pressure from the current work (bottom side) and from Ref. [33] (upper side). As expected, NS equations predict a thinner shock wave compared to the

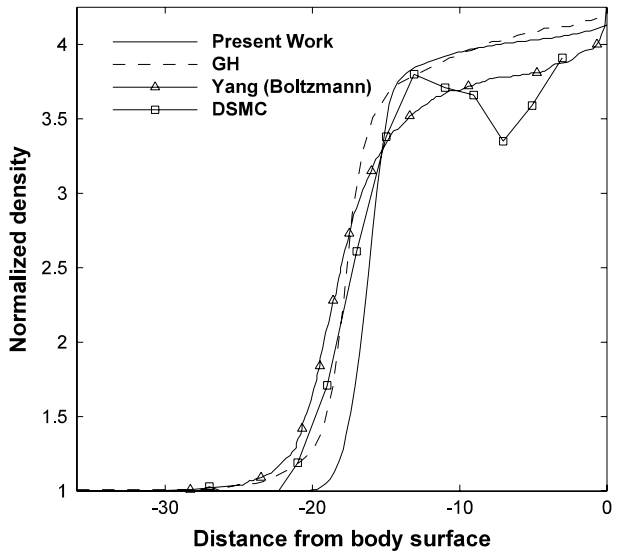

(a) Density.

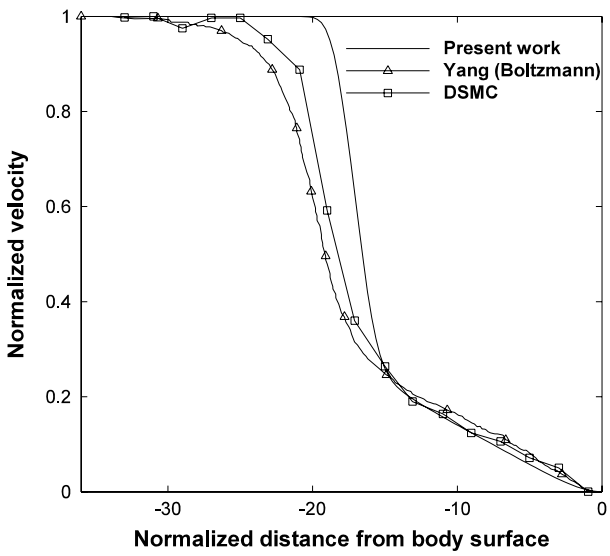

(b) Velocity.

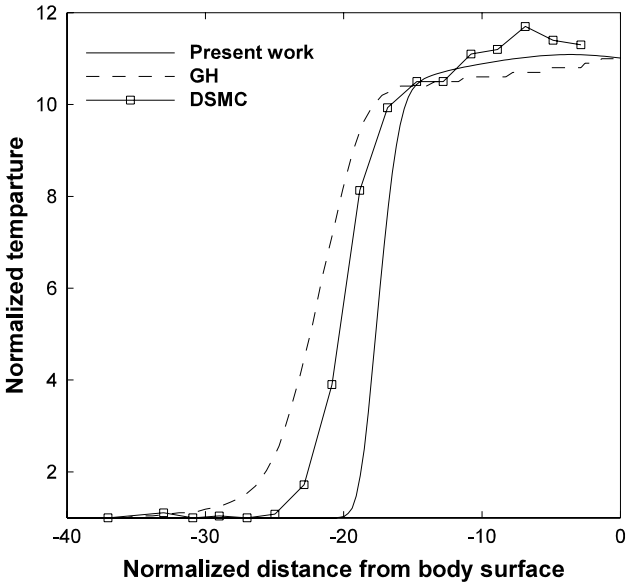

(c) Temperature.

Fig. 12. Comparison of normalized flow properties along the stagnation line between different methods.

DSMC solution while post-shock contour levels, especially in the rear portion of the cylinder, show suitable agreement with the DSMC.

The mean absolute percentage error (MAPE) for density and pressure over the whole surface of the cylinder is reported in Table 3.

$$\text{MAPE} = \frac{1}{n}\sum_{t=1}^{n}\left|\frac{X_{\text{Boltzmann}} - X_{NS}}{X_{\text{Boltzmann}}}\right|. \tag{30}$$

5. Conclusions

In the current work we extended the application of a second order slip/jump boundary conditions originally derived by Karniadakis et al. for low speed internal flows to simulate high speed rarefied flows over typical external geometries. We developed an explicit finite element solver based on the Petrov–Galerkin method and solved rarefied flow over a flat plate and a cylinder. We compared our results with the solutions of alternative BC models including Maxwell/Smoluchowski and Paterson equations. Our results show that the solution of the Karniadakis model for slip velocity of the flat plate is quite close to the DSMC solution while its temperature jump prediction is as accurate as the Paterson model. For cylinder geometry, we

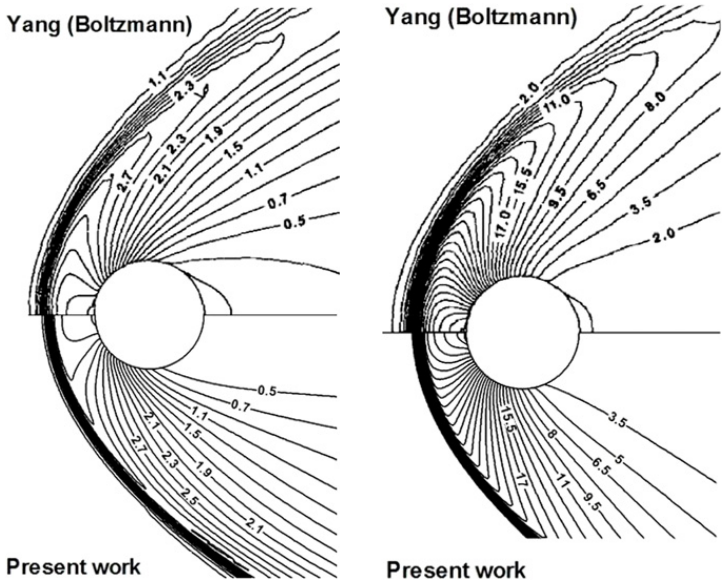

(a) Density contours. (b) Pressure contours.

Fig. 13. Hypersonic rarefied flow past a circular cylinder, comparison of the current work with Ref. [33].

Table 3
Mean absolute percentage error for density and pressure over the whole surface of the cylinder.

Contour	Density	Pressure
MAPE	12.49%	16.66%

observed that the Karniadakis model predicts post-shock properties suitably while its prediction for pressure and density contours behind the cylinder relatively agrees with the solution of the Boltzmann equation. Since the use of Karniadakis BC's does not require computation of higher order flow gradients, the numerical solver using this model is quite stable and requires less computational time.

Acknowledgment

The authors would like to acknowledge the financial supports provided by "Iranian Elite Foundation" for developing HPC laboratory under Grant No. 100720.

References

[1] M. Gad-el-Hak, Fluid mechanics of microdevices—the Freeman Scholar lecture, Trans. ASME, J. Fluids Eng. 121 (1999) 5–33.
[2] H. Struchtrup, M. Torrilhon, Regularization of Grad's 13-moment equations: derivation and linear analysis, Phys. Fluids 15 (2003) 2668.
[3] H. Struchtrup, Stable transport equations for rarefied gases at high orders in the Knudsen number, Phys. Fluids 16 (2004) 3921.
[4] H. Struchtrup, Macroscopic Transport Equations for Rarefied Gas Flows: Approximation Methods in Kinetic Theory, Springer, 2005.
[5] R. Anirudh, M. Torrilhon, H. Struchtrup, A robust numerical method for the R13 equations of rarefied gas dynamics: application to lid driven cavity, J. Comput. Phys. 236 (2013) 169–186.
[6] B.C. Eu, Generalized Thermodynamics: The Thermodynamics of Irreversible Processes and Generalized Hydrodynamics, Kluwer Academic Publishers, Dordrecht, 2002.
[7] J.C. Maxwell, On stresses in rarefied gases arising from inequalities of temperature, Philos. Trans. R. Soc. 170 (1879) 231–256. Part 1.
[8] M.V. Smoluchowski, Über wärmeleitung in verdünnten gasen, J. Ann. Phys. Chem. 64 (1898) 101–130.
[9] W.M. Zhang, G. Meng, X. Wei, A review on slip models for gas microflows, J. Microfluid. Nanofluid. 13 (2012) 845–882.
[10] S.K. Loyalka, N. Petrellis, S.T. Stvorick, Some numerical results for the BGK model: thermal creep and viscous slip problems with arbitrary accommodation of the surface, J. Phys. Fluids 18 (1975).
[11] P. Bahukudumbi, A. Beskok, A phenomenological lubrication model for the entire Knudsen regime, J. Micromech. Microeng. 13 (2003) 873–884.
[12] G.E. Karniadakis, A. Beskok, N. Aluru, Microflows and Nanoflows: Fundamentals and Simulation, Springer-Verlag, New York, 2005.
[13] A. Agrawal, S.V. Prabhu, Deduction of slip coefficient in slip and transition regimes from existing cylindrical Couette flow data, J. Exp. Therm. Fluid. Sci. 32 (2008) 991–996.
[14] R. Schamberg, The fundamental differential equations and the boundary conditions for high speed slip-flow, and their application to several specific problems (Ph.D. thesis), California Institute of Technology, 1947.
[15] S. Chapman, T.G. Cowling, The Mathematical Theory of Nonuniform Gases, third ed., Cambridge University Press, New York, 1970.
[16] D.A. Lockerby, J.M. Reese, D.R. Emerson, R.W. Barber, Velocity boundary condition at solid walls in rarefied gas calculations, J. Phys. Rev. 70 (2004).
[17] Q. Li, Y.L. He, G.H. Tang, W.Q. Tao, Lattice Boltzmann modeling of microchannel flows in the transition flow regime, J. Microfluid. Nanofluid. 10 (2011) 607–618.
[18] L. Gibelli, Velocity slip coefficients based on the hard-sphere Boltzmann equation, J. Phys. Fluids 24 (2012).

[19] B.C. Eu, R.E. Khayat, G.D. Billing, C. Nyeland, Nonlinear transport coefficients and plane Couette flow of a viscous, heat conducting gas between two plates at different temperatures, Can. J. Phys. 65 (1987) 1090–1103.
[20] R.S. Myong, A computational method for Eu's generalized hydrodynamic equations of rarefied and microscale gas dynamics, J. Comput. Phys. 168 (2001) 47–72.
[21] R.S. Myong, Gaseous slip models based on the Langmuir adsorption isotherm, J. Phys. Fluids 16 (2004) 104–117.
[22] R.S. Myong, J.M. Reese, R.W. Barber, D.R. Emerson, Velocity slip in microscale cylindrical Couette flow: the Langmuir model, J. Phys. Fluids 17 (2005).
[23] S. Vakilipour, M. Darbandi, Advancement in numerical study of gas flow and heat transfer in a microscale, J. Thermophys. Heat Transfer 23 (2009) 205–208.
[24] F.P. Brueckner, J.C. Heinrich, Petrov–Galerkin finite element model for compressible flows, J. Numer. Methods Eng. 32 (1991) 255–274.
[25] C.C. Yu, J.C. Heinrich, 'Petrov–Galerkin method for multidimensional, time-dependent, convective-diffusion equations', Int. J. Numer. Methods Eng. 24 (1987) 2201–2215.
[26] G.A. Bird, Molecular Gas Dynamics and the Direct Simulation of Gas Flows, Oxford Science, Oxford, 1994.
[27] M. Darbandi, E. Roohi, A hybrid DSMC/Navier–Stokes frame to solve mixed rarefied and non-rarefied micro/nanoflows, Internat. J. Numer. Methods Fluids 72 (2013) 937–966.
[28] T. Scanlon, E. Roohi, C. White, M. Darbandi, J. Reese, An open source, parallel DSMC code for rarefied gas flows in arbitrary geometries, Comput. & Fluids 39 (2010) 2078–2089.
[29] C.J. Greenshields, J.M. Reese, Rarefied hypersonic flow simulations using the Navier–Stokes equations with non-equilibrium boundary conditions, J. Prog. Aerosp. Sci. 52 (2012) 80–87.
[30] F.W. Vogenitz, G.A. Bird, J.E. Broadwell, H. Rungaldier, Theoretical and experimental study of rarefied supersonic flows about several simple shapes, AIAA J. 6 (12) (1968) 2388–2394.
[31] W. Wetzel, H. Oertel, Direct Monte Carlo simulations of hypersonic flows past blunt bodies, Progr. Astronaut. Aeronaut. 118 (1989) 432–446.
[32] R.S. Myong, A generalized hydrodynamic computational model for rarefied and microscale diatomic gas flows, J. Comput. Phys. 195 (2004) 655–676.
[33] J.Y. Yang, J.C. Huang, Rarefied flow computations using nonlinear model Boltzmann equations, J. Comput. Phys. 120 (1995) 323–339.
[34] T.E. Schwartzentruber, L.C. Scalabrin, I.D. Boyd, Hybrid particle–continuum simulations of non-equilibrium hypersonic blunt-body flow fields, J. Thermophys. Heat Transfer 22 (2008) 29–37.